Bending of vertical Hopf bifurcation branches in rotating thermal convection with an imperfection

Eusebius J. Doedel*

Department of Computer Science, Concordia University, Montreal, Quebec, Canada H3G 1M8

Jerry F. Magnan†

Department of Mathematics, Florida State University, Tallahassee, Florida 32306-3027

Edward L. Reiss

Department of Engineering Sciences and Applied Mathematics, Northwestern University, Evanston, Illinois 60201

The cascading bifurcation of two-dimensional, steady and periodic, thermal convection states in a rotating box with a uniform temperature distribution on the walls was studied by Magnan and Reiss, SIAM J. Appl. Math. (to be published). We extend that perturbation analysis by considering the effect of a slightly nonuniform temperature distribution on a wall of the box. This imperfection can qualitatively alter the response of the convection system. In particular, our two-parameter study finds that (a) the "vertical" Hopf bifurcation branch of periodic solutions, previously obtained at third order for a uniform temperature distribution, is now "bent" by the imperfection; (b) the number and position of the Hopf bifurcation points on the steady solution branches can vary with the strength of the imperfection and thus the stabilities of these branches can accordingly change; (c) the periodic solution branches, which now bifurcate either to the right or left, terminate in either a Hopf bifurcation point or in an infinite period bifurcation point; and (d) the imperfection can dominate the effects of higher-order terms in the amplitude equations. Furthermore, we establish for a semibounded rotating convection layer that when an imperfection is present the nonlinear interaction of two primary bifurcation steady states can generate stable, periodic solution branches, which has not been shown to occur for ordinary (nonrotating) Rayleigh-Benard convection, or for any other convection system.

I. INTRODUCTION

The cascading bifurcation of two-dimensional, steady and periodic, thermal convection states in a rotating, infinitely long, rectangular box which is uniformly heated from below is studied in Ref. 1 by perturbation methods. The sides of the box are partially stress free with thermally insulated vertical sides and perfectly conducting horizontal sides. The bifurcation points of the conduction state depend on the system parameters which are the aspect ratio of the box (l), the Prandtl number (σ), and the Taylor number (T). In that analysis[1] these parameters are restricted to ranges such that the two lowest bifurcation points correspond to two-dimensional steady states of convection (rolls). For the range of parameters selected in Ref. 1, which corresponds to a fluid such as air or liquid nitrogen ($\sigma \approx 0.7$) in a channel of square cross section ($l = 1$), the first two steady modes to become unstable have wave numbers of 1 and 2. These two modes can be made to bifurcate simultaneously from one point on the conduction state by appropriately selecting the values of two system parameters. Thus, the two modes coalesce at the critical Rayleigh number $R = R_c^0$ when $T = T_0$. Splitting of the multiple bifurcation point R_c^0 by varying T from T_0 then leads to cascading bifurcations of solutions of the convection prob-

lem; see also Refs. 2–6. Asymptotic expansions of these solutions are obtained as $\epsilon^2 \equiv T^{1/2} - T_0^{1/2} \to 0$ for R near R_c^0.

The results of that analysis show that as R is increased the system undergoes a sequence of successive bifurcations. First, the conduction state loses stability to a pure, or single, steady-state mode at the lowest bifurcation point on the conduction state. Then, this pure state loses stability to a mixed, or double, steady-state mode at a larger value of R, which corresponds to a secondary bifurcation point. Finally, the mixed state then becomes unstable at a tertiary bifurcation point R_H, which is a Hopf bifurcation point. Since the perturbation analysis in Ref. 1 is carried out to third order the branch of periodic solutions bifurcating from R_H is vertical, i.e., it exists only for $R = R_H$. Thus, as we discuss in Ref. 1 and summarize in Sec. II of this paper, if R slightly exceeds R_H then the resulting transient motion will always move far away from the tertiary bifurcation point of the vertical Hopf branch; but, for sufficiently small times which are still large compared to typical experimental observation times the solutions may appear to be either steady, or jumping between steady states (perhaps randomly), or time periodic. To "bend" the vertical branch requires either a fifth-order calculation or the addition of imperfections to the model, or both. However,

the effect of the imperfections can dominate those of the higher-order terms.

In this paper we investigate the effect of imperfections[5,7,8] on the response of the rotating convection system. In particular, we consider imperfections that are caused by a slightly nonuniform temperature distribution imposed on the top boundary of the convection box.[8] This boundary condition is more realistic than the perfectly uniform temperature distribution used in Ref. 1 and elsewhere, since thermal noise is always present in experiments. The imperfection introduces small additional (constant) terms in the amplitude equations which qualitatively change the response of the system. The convection problem with imperfections is formulated in Sec. III.

The solutions of the amplitude equations vary with the imperfection strength and R. As the former quantity is varied the number and position of Hopf bifurcation points can change (cf. Figs. 4 and 8) and as the latter is varied the system may exhibit transitions between steady states and between steady and periodic states (cf. Fig. 3). Thus, periodic solution branches may connect two Hopf bifurcation points, or they may connect a Hopf bifurcation point with an infinite period bifurcation point. Moreover, the imperfections bend the vertical branch obtained in Ref. 1 so that a transition from the mixed steady state to a stable periodic state can now occur as R exceeds R_H. A typical imperfect bifurcation diagram is given in Fig. 3, which is drawn for a particular value of the imperfection strength. The amplitude equations for the imperfect problem are obtained and their solutions discussed in Sec. IV and summarized in Sec. V.

In ordinary (nonrotating) thermal convection without imperfections the nonlinear interaction of two primary bifurcation steady states has not been shown to generate a periodic state near the primary bifurcation points.[6,9] However, it has been shown[4,10−13] that such a phenomenon is possible for a general dynamical system describing the interaction of two primary bifurcation steady states. The rotating thermal convection problem presented in Ref. 1 is a realization of such a dynamical system which exhibits a tertiary Hopf bifurcation on a mixed-mode secondary bifurcation steady state. This Hopf bifurcation branch is vertical since only cubic nonlinearities were included in the amplitude equations; but, the vertical branch can be bent by also including the quintic nonlinearities.[12] The physical mechanism for this oscillatory behavior is different from that responsible for the bifurcation of a periodic solution from the conduction state, which can occur for rotating thermal convection and other kinds of convection, but not for ordinary thermal convection. It is interesting to observe that in a rotating infinite layer a secondary Hopf bifurcation ending in an infinite period was obtained in Ref. 14 for three nonlinearly interacting steady convection states. In that case, the nonlinear interaction does not result from the "splitting" of the coalescence point of primary bifurcation points, as in the present work. Furthermore, the three-dimensional time periodic behavior is associated with the Kuppers-Lortz instability which involves three-roll states with different orientations. Thus, the work of Ref. 14 deals with a different physical phenomenon than the one considered here.

Imperfect bifurcation in ordinary thermal convection has also been previously investigated.[5,8] Two-dimensional convection in a box with slightly imperfectly insulated side walls was considered in Ref. 5 where the aspect ratio of the box was used as the bifurcation parameter. There, when two primary steady convection states interact nonlinearly the imperfection does not generate a periodic response of the system. This is in contrast to the present problem with rotation in which stable periodic bifurcation states are generated by stationary imperfections. This work theoretically derives for a rotating semibounded convection layer the generation of stable periodic states by the local nonlinear interaction of two primary bifurcation steady states.

The physical model of the convection treated here is somewhat idealized since, for example, it employs stress-free boundary conditions and treats two-dimensional convection states. However, this model not only makes the problem analytically tractable but may also give insight into the phenomenon of the generation of a periodic state by the nonlinear interaction of two steady states for physically realistic convection systems. Such a phenomenon has not been numerically or experimentally investigated in rotating thermal convection, but what appears to be a related phenomenon has been investigated experimentally in ordinary thermal convection. In that study, the transition between two steady pure mode states (a three-roll and two-roll state) was observed for a low Prandtl number fluid in a small box.[15] The results show the presence of mixed mode periodic oscillations in the transition region between the two steady modes. This periodic state, which represents a "switching" back and forth between the two pure modes, is reminiscent of periodic states described by our analysis. A theoretical explanation of the observed oscillations is currently lacking, although a start in this direction has been made.[9]

It would be interesting to study the "realistic" rotating convection problem in the parameter regime where steady states locally interact for then we could determine the degree of applicability of the results derived here for the "idealized" problem. Although studies near such a codimension-two point are currently lacking there is one study[16] which is particularly relevant to the convection problem studied here. It involves a numerical and experimental investigation of a rotating rectangular box with rigid walls containing a fluid with Prandtl number of 0.7, which corresponds to a fluid such as nitrogen gas. It was experimentally observed and numerically verified that there are values of the Taylor number for which the rolls have their axes parallel to the long side of the box. This is not the case with ordinary thermal convection where the rolls orient themselves with their axes perpendicular to the long side of the box. In addition, the results suggest that the Taylor number at which the roll orientation changes (from being perpendicular to being parallel to the long side of the box) decreases as the length of the box increases. Thus, one expects that in a very long box "parallel rolls" would be found at low

Taylor numbers, as in our idealized model. The interaction of rolls was not investigated in the study. Clearly, further work is required to compare our analytical results with experimental and numerical studies of the interaction.

II. THE PERFECT PROBLEM

The Boussinesq theory for the two-dimensional convection of a viscous, incompressible fluid contained in an infinitely long rectangular box uniformly heated from below and rotating about the vertical z axis is given in dimensionless variables by[1,17]

$$\sigma^{-1}\Delta\psi_t - \Delta^2\psi + lR\Theta_x - T^{1/2}v_z = \sigma^{-1}lJ(\psi,\Delta\psi) , \quad (2.1a)$$

$$\Theta_t - \Delta\Theta + l\psi_x = lJ(\psi,\Theta) , \quad (2.1b)$$

$$\sigma^{-1}v_t - \Delta v + T^{1/2}\psi_z = \sigma^{-1}lJ(\psi,v) , \quad (2.1c)$$

$$\psi = \psi_{zz} = \Theta = v_z = 0 \quad \text{for } z = 0,\pi \text{ and } 0 \leq x \leq \pi \quad (2.1d)$$

$$\psi = \psi_{xx} = \Theta_x = v = 0 \quad \text{for } x = 0,\pi \text{ and } 0 \leq x \leq \pi . \quad (2.1e)$$

In (2.1) ψ is the stream function, Θ the temperature, and v the y velocity component. These variables give the departure of the system from the conduction state $\psi = \Theta = v = 0$, which is a solution of (2.1). The dimensionless x and z velocity components u and w are related to the stream function by $u = \psi_z$ and $w = -l\psi_x$. In addition, l is the aspect ratio of the box, $\sigma = \nu/\kappa$ is the Prandtl number, Δ and J are defined by

$$\Delta = l^2\partial_x^2 + \partial_z^2, \quad \text{and} \quad J(f,g) = f_x g_z - f_z g_x , \quad (2.2)$$

and

$$R \equiv \frac{\alpha g d^3(T_l - T_u)}{\pi\kappa\nu}, \quad T \equiv \frac{4\Omega^2 d^4}{\nu^2} . \quad (2.3)$$

Here ν, κ, and α are, respectively, the kinematic viscosity, the thermometric diffusivity, and the coefficient of thermal expansion of the fluid. Furthermore, Ω is the uniform angular velocity of rotation of the box, πd is the height of the box, g is the gravitational acceleration, and T_l and T_u are the uniform temperatures applied to the lower and upper surfaces of the box, respectively.

These boundary conditions (2.1d) and (2.1e) imply that the horizontal walls of the convection box are stress-free and the thermally insulated vertical walls are "partially stress-free." They differ from those found in laboratory experiments. However, the solutions of the idealized convection problem (2.1) may help us to understand experimental and numerical results obtained with the more realistic rigid boundary conditions. Furthermore, the boundary conditions (2.1d) and (2.1e) have the mathematical virtue that the linearized convection theory can be explicitly solved, thus rendering the problem analytically tractable, as has been demonstrated previously.[1,17-19] We refer to the problem determined by (2.1) as the perfect problem because imperfections are not considered and we denote it as P.

Asymptotic solutions of P were obtained in Ref. 1 by restricting the system parameters l, σ, and T to ranges where the two lowest bifurcation points of the conduc-

tion state correspond to two-dimensional steady states of convection and coalesce at the critical Rayleigh number $R = R_c^0$. For simplicity we considered a square cross section $(l = 1)$, although it was not essential to make this choice, and restricted P to an interval such that the two lowest bifurcation points coalesced for $T = T_0$. Then, defining the small parameter ϵ by $T^{1/2} = T_0^{1/2} + \epsilon^2$ and using a multitime method, asymptotic expansions were obtained as $\epsilon \to 0$, of the solution of P for R near R_c^0. The splitting of the multiple bifurcation point $(R = R_c^0, T = T_0)$ of the conduction state as ϵ varies from zero then leads to secondary and cascading bifurcation in accordance with the general ideas introduced in Refs. 2–4.

The asymptotic expansion of the solution is given by

$$\psi = \epsilon[A(\tau)\phi_1 + B(\tau)\phi_2] + O(\epsilon^2) + \mathbf{E} , \quad (2.4)$$

where the three component vector $\psi \equiv (\psi,\Theta,v)$ and the eigenmodes ϕ_1,ϕ_2, which become unstable at $R = R_c^0$, are given by

$$\phi_1 = \begin{bmatrix} \dfrac{-(1+l^2)}{T_0^{1/2}}\sin(x)\sin(z) \\[2mm] \dfrac{l}{T_0^{1/2}}\cos(x)\sin(z) \\[2mm] l\sin(x)\cos(z) \end{bmatrix} , \quad (2.5a)$$

$$\phi_2 = \begin{bmatrix} \dfrac{-(1+4l^2)}{T_0^{1/2}}\sin(2x)\sin(z) \\[2mm] \dfrac{2l}{T_0^{1/2}}\cos(2x)\sin(z) \\[2mm] l\sin(2x)\cos(z) \end{bmatrix} . \quad (2.5b)$$

These modes represent one-roll and two-roll states, respectively, and, are the *first* to become unstable at $R = R_c^0$ for the range of parameters considered.[1] In (2.4) $\tau \equiv \epsilon^2 t$ is a slow time and $\mathbf{E}$ represents terms which are exponentially decaying in the fast time t. The slowly varying amplitudes $A(\tau)$ and $B(\tau)$ satisfy the following pair of coupled ordinary differential equations with cubic nonlinearities:

$$\dot{A} = A[a_1(r) + a_2 A^2 + a_3 B^2] , \quad (2.6a)$$

$$\dot{B} = B[b_1(r) + b_2 B^2 + b_3 A^2] . \quad (2.6b)$$

The coefficients a_i and b_i, $i = 1,2,3$, in (2.6) are defined in the Appendix. Moreover, the overdots denote derivatives with respect to τ, and r is a free parameter defined by the expansion of the bifurcation parameter R,

$$R = R_c^0 + r\epsilon^2 + O(\epsilon^2) . \quad (2.7)$$

Thus R is varied by changing r.

In Ref. 1 and here, our results are restricted to values of the system parameters l and σ (and hence T_0 and R_c^0) for which (a) the two lowest modes that coalesce (at $T = T_0$, $R = R_c^0$) are the $m_1 = 1$ and $m_2 = 2$ steady modes, and (b) the first and second modes to bifurcate as R increases are supercritical and subcritical, respectively, for $T - T_0$ small and positive. If we choose $l = 1$ (a

square cross section) then, as discussed in Ref. 1, our results apply for the range $0.590 < \sigma < 0.892$. In this range the $m_2 = 2$ mode is supercritical and the $m_1 = 1$ mode is subcritical. In this work we consider the specific case $l = 1$ and $\sigma = 0.8$; and, thus, the two interacting modes coalesce at $T_0 = 31$ and $R_c^0 = 39$. All of the figures have been drawn for this specific case. The bifurcation of the solutions of (2.6) and their stabilities are shown in Fig. 1. Solid (dashed) curves indicate stable (unstable) solutions in Figs. 1(b) and 1(c). Figure 1(a) shows the numerically calculated three-dimensional bifurcation diagram, and Figs. 1(b) and 1(c) show two schematic bifurcation diagrams which represent the projections on the A,R and B,R planes. This figure is analogous to Fig. 3 of Ref. 1. For $R < R_{21}^s$ ($R > R_{21}^s$), the conduction state, which corresponds to $A = B = 0$, is stable (unstable). Primary bifurcation of pure B steady states, for which $A = 0$, occurs at $R = R_{21}^s$. These states are stable for $R_{21}^s < R < R_{21}^\sigma$ and unstable for $R > R_{21}^\sigma$. Secondary bifurcation of mixed A and B steady states, for which $A \neq 0$ and $B \neq 0$, occurs at $R = R_{21}^\sigma$. The mixed states exist for $R_{21}^\sigma < R < R_{11}^\sigma$ and they are stable for $R_{21}^\sigma < R < R_H$ and unstable for $R_H < R < R_{11}^\sigma$. The tertiary bifurcation at $R = R_H$ is a time periodic solution so that R_H is a Hopf bifurcation point. Tertiary Hopf bifurcation occurs whenever the first interacting steady state to become unstable bifurcates supercritically and the second subcritically.[4,10–13] This Hopf bifurcation is degenerate (and is called a vertical Hopf bifurcation) because there is a one-parameter family of periodic solutions bifurcating from $R = R_H$ which exists *only* at $R = R_H$. This family of limit cycles is obtained from the first integral of (2.6) at $R = R_H$, as shown in the phase plane diagram of Fig. 2. The "energy" of the system, which depends on the initial conditions for (2.6), determines each curve in the family. The period of the limit cycles increases from a known finite value at the center (A_H, B_H), where the periodic solutions bifurcate, to an infinite value at the heteroclinic trajectory which connects the saddle points $(0, \overline{B})$, $(\overline{A}, 0)$, and $(0,0)$. The vertical branch bends when either higher-order (quintic) terms are brought into the amplitude equations (2.6) or when "imperfections" are added to the convection problem. In this paper we employ imperfections to bend the vertical branch and, thus, introduce constant terms into (2.6).

We now summarize the main features of the transient response of the system for R in the neighborhood of R_H. The center (A_H, B_H) becomes an unstable spiral point (A_H^+, B_H^+) for R slightly greater than R_H, i.e., at $R = R_H^+ > R_H$, as shown in Fig. 5 of Ref. 1. Thus, trajectories which begin near the spiral point, i.e., close to the unstable mixed steady-state branch, spiral out and unwind in such a way that the system exhibits relaxation oscillations of $A(\tau)$ and $B(\tau)$. After a sufficiently long time has elapsed the trajectories leave the neighborhood of (A_H^+, B_H^+) and $A \to \infty, B \to 0$. Thus, every trajectory which begins near the focus eventually escapes from it and becomes unbounded. Since the escape time is large our asymptotic solution has a large range of validity. The relaxational character of the oscillations is caused
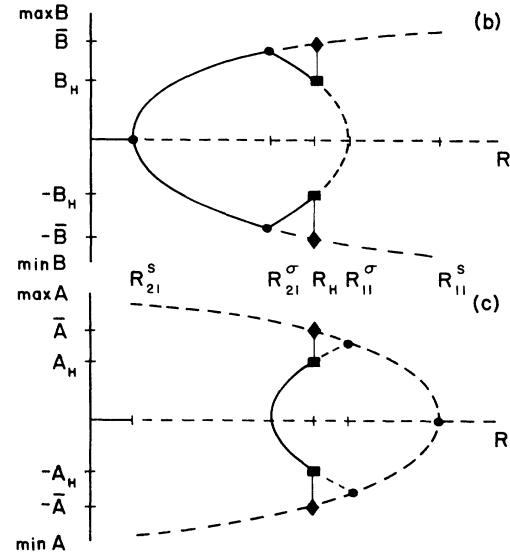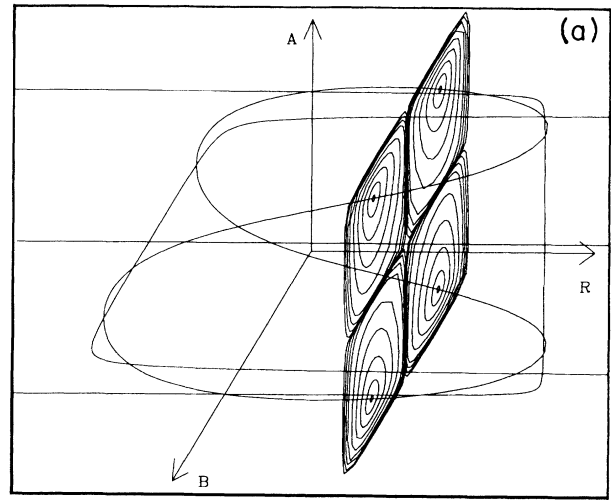

FIG. 1. Bifurcation diagrams for the solutions (A,B,R) of the amplitude equations (2.6) of the "perfect" problem. In (a) we show the numerically calculated three-dimensional bifurcation diagram where the four one-parameter families of "vertical" periodic solutions are seen to bifurcate from the mixed steady states. In (b) and (c) we show two schematic projections of the diagram in (a). We plot max B and min B vs R in (b), and max A and min A vs R in (c), to emphasize the symmetry of the periodic branches. In (b) and (c), solid (dashed) heavy lines denote the stable (unstable) steady states; and, the light vertical lines denote the vertical branches of neutrally stable periodic states. The pure and mixed steady states are labeled by the letters p and m, respectively. Steady ($\bullet$), Hopf ($\blacksquare$), and infinite period ($\blacklozenge$) bifurcation points are also indicated. The vertical, periodic branch of solutions begins at (A_H, B_H, R_H) and ends at $(\overline{A}, \overline{B}, R_H)$, cf. Fig. 2. In (a)–(c) $\sigma = 0.8$, $l = 1$, and $\epsilon = 0.1$. In (b) and (c) $R_{21}^s = 39.027\,839$, $R_{21}^\sigma = 39.028\,089$, $R_H = 39.082\,266$, $R_{11}^\sigma = 39.113\,05$, and $R_{11}^s = 39.111\,355$; $\overline{A} = 6.182\,226$, $\overline{B} = 1.369\,729$, $A_H = 0.207\,503$, $B_H = 0.054\,901$, max $A (R_{11}^\sigma) = 0.257\,169$, and max $B (R_{21}^\sigma) = 0.092\,939$.
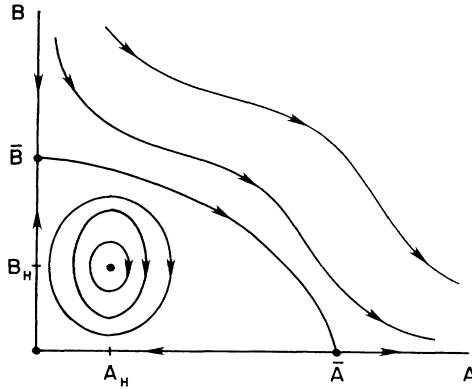
FIG. 2. Phase plane diagram for the amplitude equations (2.6) at $R = R_H$. The limit cycles represent a one-parameter family of periodic solutions and correspond to the vertical periodic branches in Fig. 1. The center at (A_H, B_H) is the tertiary Hopf bifurcation point on the mixed steady-state branches. The saddle points at $(0,0)$, $(0,\bar{B})$, and $(\bar{A},0)$ represent the unstable conduction state and pure steady states, respectively. They are connected by a heteroclinic trajectory. The solutions become unbounded outside the separatrix which connects $(0,\bar{B})$ and $(\bar{A},0)$. The arrowheads indicate the direction of the flow along the trajectories. Only one quadrant is shown since the phase plane is symmetric with respect to the origin. The system parameter values are the same as in Fig. 1.

by the passage of a trajectory near the three saddle points at $(\bar{A}^{+},0)$, $(0,0)$, and $(0,\bar{B}^{+})$, and the connecting separatrices, which are all shown in Fig. 5 of Ref. 1. Thus, a trajectory which leaves the neighborhood of $(\bar{A}^{+},0)$ slows down as it approaches $(0,0)$ and similarly, when leaving the neighborhood of $(0,0)$, it speeds up as it approaches $(0,\bar{B}^{+})$. However, a trajectory speeds up considerably more in between $(0,\bar{B}^{+})$ and $(\bar{A}^{+},0)$. Thus, the flow of the system trajectory is slow near the saddle points and their connecting separatrices and fast between the two saddle points not at the origin. As a trajectory unwinds it gets closer to the saddle points and connecting separatrices with the result that the trajectory moves increasingly faster between $(0,\bar{B}^{+})$ and $(\bar{A}^{+},0)$, and increasingly slower otherwise. We find a related type of behavior for the imperfect problem in Sec. IV.

After "escape," the final state of the system cannot be described by our asymptotic analysis, so that it is not uniformly valid in τ as $\tau \to \infty$. Instead of modifying the asymptotic method to account for this nonuniformity we modify the problem, i.e., make it more realistic, by including system imperfections. The solutions of the resulting, modified amplitude equations are more complex, as we discuss in Secs. IV and V. Thus, for example, a previously vertical Hopf branch is now bent to the right for sufficiently small imperfections so that bifurcation occurs as R increases above R_H.

III. THE IMPERFECT PROBLEM

Imperfections are always present in real systems and thus any realistic theory must include them. As an im-

perfection, we modify the thermal boundary condition on the top face of the convection box by imposing a slightly nonuniform temperature distribution there, such as is done in Ref. 8 for ordinary convection near simple, critical Rayleigh numbers. Thus, the imperfect boundary condition is

$$\Theta(x,\pi) = \delta \pi f(x) \quad \text{for } 0 \le x \le \pi \tag{3.1}$$

which replaces the corresponding homogeneous condition at $z = \pi$ in (2.1d). Here, the small parameter δ is the amplitude of the imperfection and $f(x)$ is its distribution. We require that the compatibility conditions $f'(0) = f'(\pi) = 0$ are satisfied by $f(x)$ because of the Θ boundary condition in (2.1e) on the sides of the box. We relate the two small parameters δ and ϵ by $\delta = \epsilon^3$ in accordance with the general theory of imperfect bifurcation.[7] Then, as we show, the resulting amplitude equations are a modification of the amplitude equations (2.6) of the perfect problem. The imperfect convection problem thus consists of (2.1) with (3.1) replacing the inhomogeneous boundary condition on Θ in (2.1d).

It is convenient for the analysis of the imperfect problem to have homogeneous boundary conditions. Thus we define a reduced temperature $\hat{\Theta}$ by

$$\hat{\Theta}(x,z) = \Theta(x,z) - \epsilon^3 f(x)z \ . \tag{3.2}$$

Then, the imperfect problem, which we denote by I, is given by

$$\sigma^{-1}\Delta\psi_t - \Delta^2\psi + lR\,\hat{\Theta}_x - T^{1/2}v_z + \epsilon^3 lRf''z$$
$$= \sigma^{-1}lJ(\psi, \Delta\psi) \ , \tag{3.3a}$$

$$\hat{\Theta}_t - \Delta\hat{\Theta} + l\psi_x - \epsilon^3 l^2 f''z = lJ(\psi, \hat{\Theta}) + \epsilon^3 lJ(\psi, fz) \ , \tag{3.3b}$$

$$\sigma^{-1}v_t - \Delta v + T^{1/2}\psi_z = \sigma^{-1}lJ(\psi, v) \ , \tag{3.3c}$$

$$\psi = \psi_{zz} = \hat{\Theta} = v_z = 0 \quad \text{for } z = 0, \pi \text{ and } 0 \le x \le \pi \tag{3.4a}$$

$$\psi = \psi_{xx} = \hat{\Theta}_x = v = 0 \quad \text{for } x = 0, \pi \text{ and } 0 \le z \le \pi \ . \tag{3.4b}$$

If $f(x) \equiv 0$, then I reduces to P.

IV. SOLUTIONS OF THE AMPLITUDE EQUATIONS

We obtain an asymptotic expansion of the solution of I as $\epsilon \to 0$ by the multitime method as we did in Ref. 1 for P. We omit all the details of the calculations since they are straightforward, but lengthy. The solution is given by (2.4) where the slowly varying amplitudes $A(\tau), B(\tau)$ satisfy the amplitude equations,

$$\dot{A} = A[a_1(r) + a_2 A^2 + a_3 B^2] + I_A \ , \tag{4.1a}$$

$$\dot{B} = B[b_1(r) + b_2 B^2 + b_3 A^2] + I_B \ . \tag{4.1b}$$

Here, the constants I_A and I_B, which are defined in the Appendix, are functions of $f'(x)$ and $f''(x)$. To simplify the discussion of the solutions of (4.1) we specifically choose

$$f(x) \equiv \alpha \cos(2x) \ , \tag{4.2}$$

where α is a constant. With this imperfection distribution we obtain

$$I_A = 0 \ , \tag{4.3a}$$

$$I_B = \alpha I \ , \tag{4.3b}$$

where I is a constant, which is obtained from (A19)–(A21) in the Appendix and (4.2). We obtain (4.3) if $f(x)$ is an even function with respect to $\pi/2$. In addition, if $f(x)$ is odd with respect to $\pi/2$ then $I_A \neq 0$ and $I_B = 0$; and, if $f(x)$ is neither even or odd with respect to $\pi/2$ then $I_A \neq 0$ and $I_B \neq 0$. We consider all these cases and, thus, a general perturbation. The steady and periodic solutions of the amplitude equations (4.1) with (4.3) were numerically evaluated and plotted using the computer software package AUTO.[20,21] The steady solutions of the amplitude equations (4.1) with (4.3) for the pure steady state are given by

$$A = 0 \ , \tag{4.4a}$$

$$B^3 + \frac{b_1(r)}{b_2} + B + \frac{\alpha I}{b_2} = 0 \ ; \tag{4.4b}$$

and for the mixed steady states,

$$A^2 = -\frac{a_1(r) + a_3 B^2}{a_2} \ , \tag{4.5a}$$

$$B^3 + \frac{a_2 b_1(r) - b_3 a_1(r)}{a_2 b_2 - a_3 b_3} B + \frac{\alpha a_2 I}{a_2 b_2 - a_3 b_3} = 0 \ . \tag{4.5b}$$

The bifurcation diagram is now more complicated than for P because the steady states (4.4) and (4.5) depend on both r and α. Figure 3 shows the steady states calculated from (4.4) and (4.5) for $\alpha = \alpha_1 \equiv 1.0 \times 10^{-5}$. The three-dimensional bifurcation diagram is shown in Fig. 3(a). Its projection on the A,R and B,R planes are shown schematically in Figs. 3(b) and 3(c), respectively. For clarity, the pure and mixed steady states are labeled by the letters p and m, respectively.

There is one pure steady state for $R < R_\alpha$ and three for $R > R_\alpha$. They are the perturbations of the "perfect" pure B state in problem P. They are shown in Fig. 3(b) and correspond to $A = 0$. There are no imperfect pure A states in this case; but, there are for $I_A \neq 0$, $I_B = 0$. In addition, there is one pair of mixed steady states for $R < R_\beta$, two pairs for $R_\beta < R < R_\gamma$, three pairs for $R_\gamma < R < R_\delta$, and none for $R > R_\delta$. Each pair is symmetric with respect to a reflection across the $A = 0$ plane. These mixed steady states are the perturbations of the perfect mixed steady states. Since $R_\alpha < R_\beta < R_\gamma < R_\delta$ there can be either three, five, seven, or nine imperfect steady states, depending on the value of R.

The linearized stability of the imperfect steady states is determined in the usual way by linearizing the amplitude equations (4.1) about each steady state and then solving the resulting system of two, first-order, ordinary differential equations. This establishes the stabilities, which are shown in Fig. 3(b) and Fig. 3(c), with respect to (infinite) two-dimensional rolls with axes along y. In Appendix B of Ref. 1 we show, by simple arguments, that two-dimensional rolls with axes along x as well as some three-dimensional states are not solutions of the
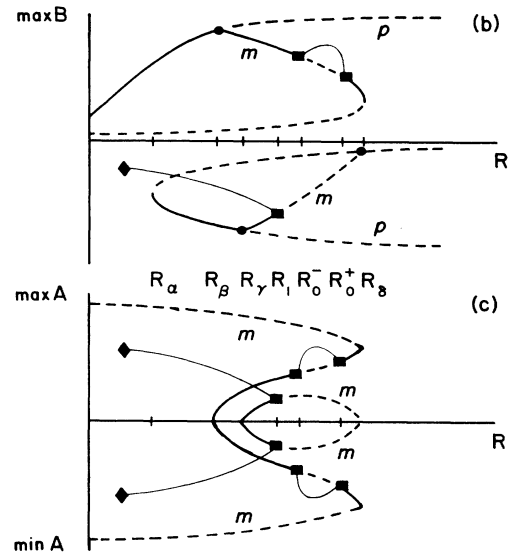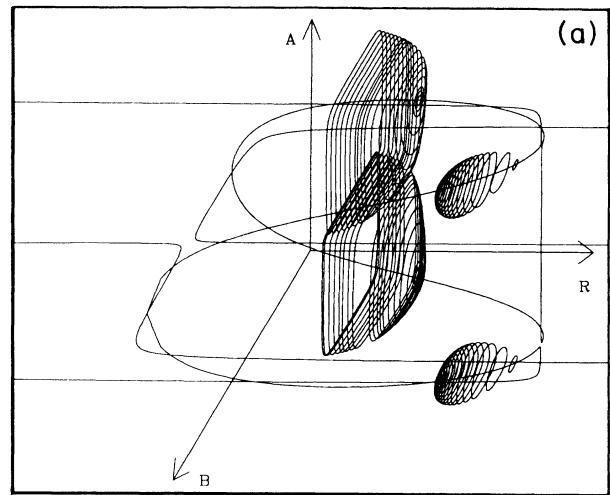

FIG. 3. Bifurcation diagrams for the solutions (A,B,R) of the "imperfect" amplitude equations (4.1) and (4.3) for $\alpha = 1.0 \times 10^{-5}$. In (a) we show the numerically calculated three-dimensional bifurcation diagram where four periodic solutions branches are seen to bifurcate from the mixed steady state. In (b) and (c) we show two schematic projections of the diagram in (a). In (b) we plot max B vs R and each point on a branch represents the two solutions, (A,B) and $(-A,B)$, with reflection symmetry. In (c) we plot max A and min A vs R for $A > 0$, respectively, to emphasize the symmetry of the periodic branches. In (b) and (c), heavy (light) lines denote steady (periodic) states and solid (dashed) lines represent stable (unstable) states. The pure and mixed steady states are labeled by the letters p and m, respectively. Steady (●), Hopf (■), and infinite period (◆) bifurcation points are also indicated. There are limit points at R_α and R_δ. The system parameter values are the same as in Fig. 1.
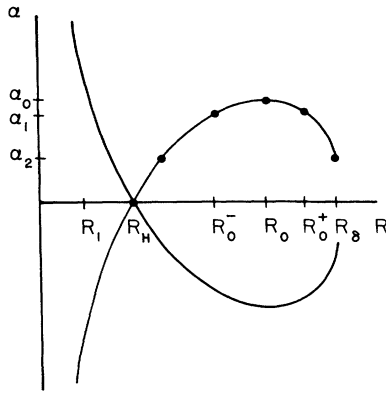
FIG. 4. Curves of Hopf bifurcation points. For $\alpha \neq 0$, each point (R,α) on the curve represents a pair of Hopf bifurcation points because of the reflection symmetry of the bifurcation diagram, cf. Fig. 3(b). Two pairs of Hopf bifurcation points coalesce at (R_0,α_0). At $\alpha=\alpha_1$ there are three pairs of Hopf bifurcation points, as shown in the bifurcation diagram of Fig. 3. As $\alpha \to \alpha_2$, $R_0^+ \to R_\delta$ so that a Hopf pair moves to the limit points of the steady branches and thus becomes a pair of infinite period bifurcation points corresponding to homoclinic orbits. The curves intersect at $(R_H,0)$ where four individual pairs, two for $\alpha > 0$ and $\alpha < 0$, become two double pairs. For $\alpha = 0$ the bifurcation diagram is reduced to Fig. 1. The system parameter values are the same as in Fig. 1.

linearized, steady-state problem corresponding to (2.1) and thus cannot occur in our convection model. In addition to the bifurcation of steady states there are bifurcations of periodic states of Hopf bifurcation points. They occur in Fig. 3 at R_0^-, R_0^+, and R_1. Furthermore, we find that depending on the value of α there can be either two, four, or six Hopf bifurcation points. This is shown by the diagram in Fig. 4 which gives the location of the pair of Hopf bifurcation points in α, R parameter space. The parameter value $\alpha=\alpha_1$, for which Fig. 3 is drawn, thus corresponds to the case where there are three pairs of Hopf bifurcation points. In Fig. 3(b), two of the pairs are at R_0^- and R_0^+ on the *upper* $(B > 0)$ pair of mixed steady-state branches while the other pair is at R_1 on the *lower* $(B < 0)$ pair of mixed steady-state branches.

The solutions of I for $\alpha=\alpha_1$ change in the following way as R is increased from R_c^0, cf. Figs. 3(b) and 3(c). The system is first in the stable, pure steady state for $R < R_\beta$. As R exceeds R_β this state becomes unstable and there is a bifurcation of a pair of stable mixed steady states. The system thus makes a transition to one of these states, which one depends on the initial conditions, and remains in that state until R reaches the first Hopf bifurcation point on this branch at $R=R_0^-$. When R exceeds R_0^- the mixed steady states become unstable and the system bifurcates to a pair of stable, time periodic solution branches. At $R=R_0^-$, the frequency of oscillation is $\omega^-(\alpha_1) \neq 0$. As R is increased further, the system exhibits oscillations of a monotonically increasing period and with an amplitude which first increases to a maximum and then decreases to zero at the second Hopf

bifurcation point, located at $R=R_0^+$ on the pair of mixed steady-state branches. At this Hopf point and for $\alpha_0 > \alpha > \alpha_2$, cf. Fig. 4, the period $\omega^+(\alpha)$ is finite with $\infty > \omega^+(\alpha) > \omega^-(\alpha)$. As R exceeds R_0^+ there is a bifurcation to the mixed steady states which have now regained their stability. They remain stable up to the limit point at $R=R_\delta$, where the branch turns back and continues for $R < R_\delta$. For $R > R_\delta$ there are no nearby stable states described by our solutions to the problem. Presumably, for $R > R_\delta$ there is a jump transition to another solution branch.

We now discuss the pair of branches of periodic solutions which exist for $R_0^- \leq R \leq R_0^+$, i.e., between the two Hopf bifurcation points on the mixed steady branches. The interval of R for which these branches of periodic solutions exist changes with α since $R_0^- = R_0^-(\alpha)$ and $R_0^+ = R_0^+(\alpha)$. We observe in Fig. 4 that for $\alpha > \alpha_0$ there are no Hopf bifurcation points on the mixed steady-state branches with $B > 0$. However, for $\alpha=\alpha_0$ and $R=R_0$ there is a pair of Hopf bifurcation points. At $\alpha=\alpha_0$ the periodic branches have shrunk to points. For a smaller value of α, say $\alpha=\alpha_1$, there are two pairs of Hopf bifurcation points. In this case, and for $\alpha_2 < \alpha < \alpha_0$, two Hopf points on the same steady branch are connected by a periodic branch. The limit cycles this time have nonzero amplitude except at the endpoints of the period branches at R_0^- and R_0^+. Therefore, we observe that the interval of R for which these periodic solutions exist increases from zero at $\alpha=\alpha_0$ to a maximum finite value at $\alpha=\alpha_2$. In addition, at every point along the branches the period increases both for fixed R as α decreases and for fixed α as R increases. Furthermore, since $\omega^+(\alpha)$ decreases from a finite value at $\alpha=\alpha_0$ to zero at $\alpha=\alpha_2$ (which defines α_2), the period of the limit cycles increase monotonically to ∞ as R increases for $\alpha=\alpha_2$. Thus, the period of the limit cycles becomes infinite as $\alpha \to \alpha_2$ and $R \to R_0^+$.

We may better understand the periodic solutions by looking at Figs. 5 and 6. In Fig. 5(a) we graph, in the max B,R plane, the periodic branch of solutions and the mixed steady-state branch for α slightly greater than α_2. In Fig. 5(b) we show a phase plane plot for a series of points along the periodic branch. This plot is continued in Fig. 5(c) with a different scale. We observe from these figures that first the amplitude of the limit cycles increases rapidly (almost vertically) from zero at R_0^- and after reaching a maximum value then decreases to zero at R_0^+. The period increases along the branch because the limit cycles are approaching a saddle point at the "nose" of the mixed steady-state branch, located at $R=R_\delta$. This saddle point is on the A axis in Fig. 5(b) and 5(c). Therefore, for $\alpha=\alpha_2$ and $R=R_\delta$, the limit cycle becomes a homoclinic orbit passing through this saddle point and thus its period is infinite. The small limit cycle in Fig. 5(c) is nearly homoclinic and thus has a very large period.

As α is decreased from α_2 we see from Fig. 4 that R_0^-, the first bifurcation point on the upper mixed steady-state branch, moves left towards $R=R_H$ which is the vertical Hopf bifurcation point of P. Thus as $\alpha \to 0$ we
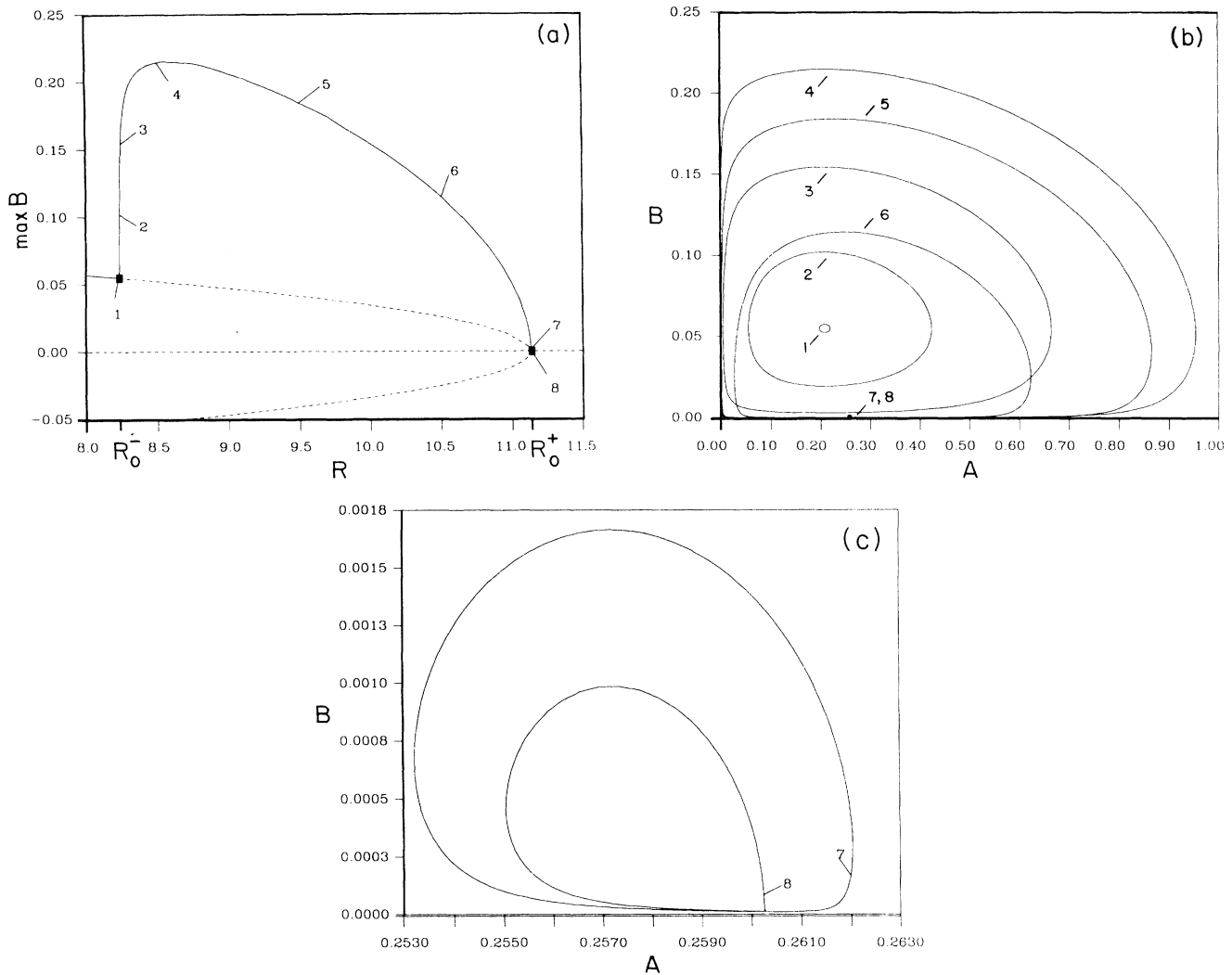
FIG. 5. Periodic solution branch for $\alpha = 5.70 \times 10^{-8}$. The bifurcation diagram, max$B$ vs R, in (a) shows the bifurcation of the periodic branch from the mixed steady-state branch for α slightly greater than α_2, cf. Fig. 4. Hopf bifurcation points are located at R_0^- and at R_0^+, which is close to the limit point R_8. Notice that the periodic branch is steep and almost vertical near R_0^-. The phase plane diagrams in (b) and (c) show the limit cycles for a series of eight points along the periodic branch. The last two points (7 and 8) on the branch are shown in (c) with an expanded scale. They correspond to limit cycles which are close to homoclinic orbits and thus have a relatively large period compared to the first six points. Near R_0^- the limit cycle oscillations are harmonic, but near R_0^+ they are relaxational because the trajectories pass near to a saddle point on the axis at $A \cong 0.26$. The system parameter values are the same as in Fig. 1.

find $R_0^- \rightarrow R_H$. For $\alpha < \alpha_2$, no second set of Hopf bifurcation points exist on the upper mixed steady-state branches in Fig. 3(b). Instead, the branches of periodic solutions terminate with infinite period, homoclinic orbits. These homoclinic trajectories pass through saddle points located on the unstable, upper mixed steady-state branches with $B \ll 1$, $A \neq 0$, and $R < R_8$. One saddle point is at $A > 0$ and the other at $A < 0$. In Fig. 6(a) we show a segment of the unstable, upper mixed steady-state branch for a value of $\alpha < \alpha_2$ which is 57 times smaller than the value of α in Fig. 5. Also shown in a segment of the stable branch of limit cycles which terminates on the steady state branch with an infinite

period bifurcation. The period at a point close to the steady-branch is large because of the homoclinic termination point of the branch. In Fig. 6(b) we show a limit cycle which is close to the homoclinic orbit. Notice the proximity of the trajectory to the A axis, where there is a saddle point which slows the flow down. The resulting time response of the system is relaxational, and is shown in Fig. 7. The response gets even "sharper" near the homoclinic point with decreasing α.

Above we have considered in detail the effect of perturbations of the form $I_A = 0$, $I_B \neq 0$ in (4.1). In addition, we have investigated perturbations of the form $I_A \neq 0$, $I_B = 0$ and $I_A \neq 0$, $I_B \neq 0$. The effect of such per-
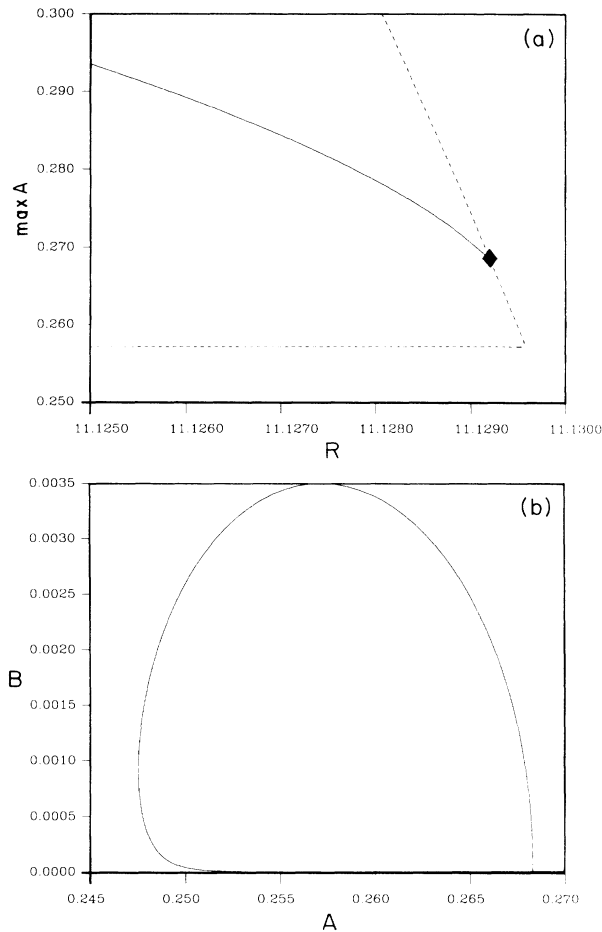
FIG. 6. Bifurcation and phase plane diagrams for $\alpha = 1.0 \times 10^{-9}$. This value of $\alpha < \alpha_2$ is 57 times smaller than the value used in Fig. 5. In (a) we plot $\max A$ vs R and graph a segment of the upper ($A > 0$, $B > 0$) mixed steady state and periodic branch. The dashed (solid) line denotes the unstable steady (stable periodic) solution branch. As the homoclinic bifurcation point ($\blacklozenge$) is approached, the period along the periodic branch becomes infinitely large. In (b) we plot the phase plane for a limit cycle which is close to the homoclinic termination point of the periodic branch and has a large but finite period. The trajectory of the limit cycle passes close to a saddle point on the A axis. The system parameter values are the same as in Fig. 1.

turbations was found to be qualitatively similar to the behavior described for $I_A = 0$, $I_B \neq 0$. In Fig. 8 we show how the Hopf bifurcation points depend on both α_A and α_B, where $I_A = \alpha_A I$, $I_B = \alpha_B I$, and I is constant. The central curve, which corresponds to $\alpha_A = 0$, also appears in Fig. 4. The curves in Fig. 8 indicate how the location and number of the Hopf bifurcation points change with α_A and α_B. We have also obtained the complete bifurcation diagrams for various values of α_A and α_B corresponding to perturbations with $I_A \neq 0$, $I_B = 0$ and with $I_A \neq 0$, $I_B \neq 0$. We find that the diagrams are similar to those with $I_A = 0$, $I_B \neq 0$. In particular, the vertical Hopf branches are bent in much the same ways in all
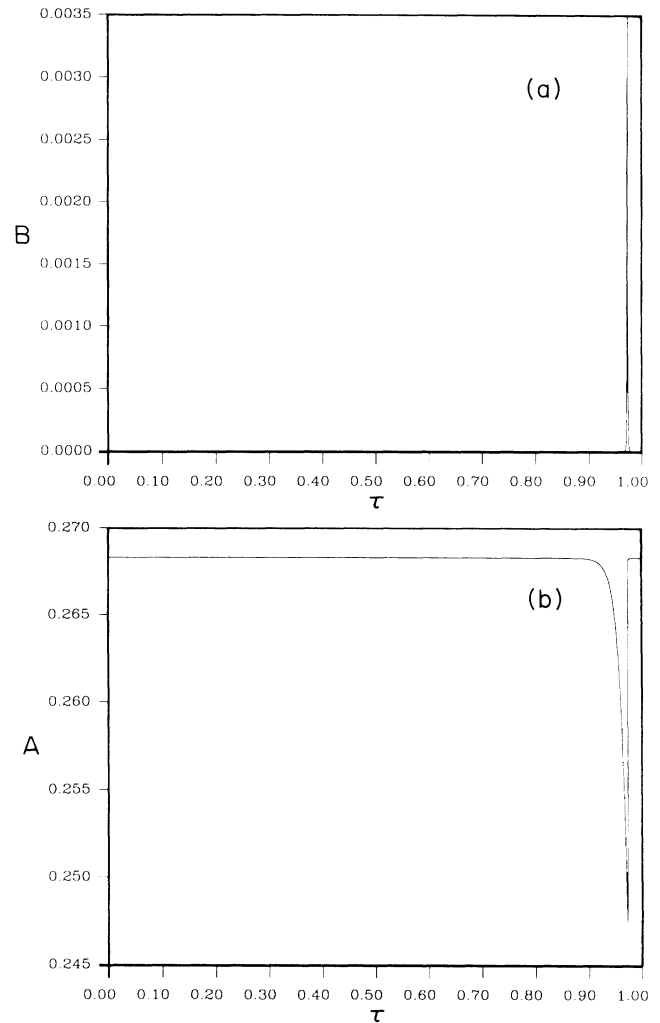

FIG. 7. Slow-time response of the amplitudes for the limit cycle shown in Fig. 6(b), which is near a homoclinic point on the periodic branch. The large period of the relaxation oscillations is normalized to 1. The system parameter values are the same as in Fig. 1.

three cases. Thus, we find that each case contains all the phenomena found in the other two. Since each case is representative of the others, we omit here the details of a general perturbation.

V. DISCUSSION OF RESULTS

We have shown for the imperfection problem that depending on the value of α, there can be either one, two, or three pairs of Hopf bifurcation points on the mixed steady-state branches, as shown in Fig. 4. We now consider and summarize these three cases and discuss the various possible states of the system as R is increased.

For $\alpha > \alpha_0$ there is one pair of Hopf points on the lower mixed steady-state branches (see Fig. 3) but none on the upper mixed steady-state branches. As R is increased from R_c^0, the system, which is initially in the pure B steady convection state, first makes a transition
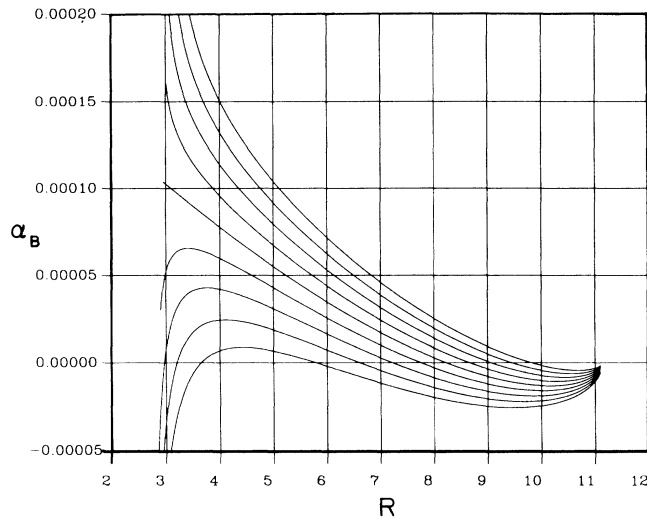
FIG. 8. Curves of Hopf bifurcation points of (4.1) for various values of α_A and α_B. From top to bottom, these curves have the values $\alpha_A = 8 \times 10^{-5}$, 6×10^{-5}, 4×10^{-5}, 2×10^{-5}, -2×10^{-5}, -4×10^{-5}, -6×10^{-5}, and -8×10^{-5}. The center curve, for which $\alpha_A = 0$, also appears as one of the two curves in Fig. 4. All the curves come in pairs that are symmetric with respect to the R axis, as in Fig. 4, but only one of each pair is shown. The system parameter values are the same as in Fig. 1.

to one of the pair of stable mixed steady convection states at $R = R_\beta$. The system remains in this state until $R = R_\delta$, where it must make a jump to a relatively large amplitude state not found in our local description of the solution to I. There is a stable segment of the pure B steady state for $R_\alpha < R < R_\gamma$ and of the pair of mixed steady states for $R_\gamma < R < R_1$, both of which occur for $B < 0$. There is also a pair of stable branches of limit cycles bifurcating from the pair of Hopf points located on the lower ($B < 0$) mixed steady-state branches at $R = R_1$. These branches, which bifurcate to the left, terminate in homoclinic orbits of infinite period and finite amplitude. The homoclinic orbit passes through a saddle point on the unstable, lower, pure B steady-state branch. The system may jump to the aforementioned lower stable states from the stable, upper mixed steady-state branch if sufficiently large perturbations are properly applied.

For $\alpha_2 < \alpha < \alpha_0$ there are three pairs of Hopf bifurcation points. Two of these pairs are on the upper mixed steady-state branches while the remaining pair is on the lower mixed steady-state branches. In this case, the behavior of the system differs from the previous one primarily because of the upper two pairs of Hopf bifurcation points. As R is increased from R_α, the system makes a transition to a periodic branch of solutions, at $R = R_0^-$, where the first pair of Hopf bifurcation points is located. Along this periodic branch, which appears at $\alpha = \alpha_0$, the period increases monotonically to a finite value at the termination point R_0^+ of the branch, which occurs at the second pair of Hopf bifurcation points. By further increasing R the system returns to the stable, mixed steady-state branch. Beyond $R = R_\delta$ the system

must jump to a large amplitude state. As $\alpha \to \alpha_2$ then $R_0^+ \to R_\delta$ and the period of the solutions at the second pair of Hopf bifurcation points becomes infinite since the limit cycles have become homoclinic orbits.

For $0 < \alpha < \alpha_2$ there are two pairs of Hopf bifurcation points. One pair is on the upper, mixed steady-state branches at $R = R_0^-$ and the other is on the lower, mixed steady-state branch at $R = R_1$. In this case, the behavior of the system differs from the previous one because there is no longer a second Hopf bifurcation point on the upper mixed steady-state branch. Instead, the periodic branch terminates in a homoclinic orbit which passes through a saddle point on the unstable, upper mixed steady-state branch with $R < R_\delta$, $B \ll 1$, and either $A > 0$ or $A < 0$. Thus, the period of the limit cycles increases from a finite value at R_0^- to an infinite value at the branches termination. The homoclinic orbit increases in amplitude as $\alpha \to 0$ and it approaches the heteroclinic orbit of P. As $\alpha \to 0$ then $R_0^- \to R_H$ and the bent periodic branches straighten up and become vertical. Similarly, the periodic branch bifurcating from the lower mixed steady-state branches which also terminate in homoclinic orbits of infinite period, become vertical as $\alpha \to 0$. This occurs as the Hopf point $R_1 \to R_H$, and as the homoclinic termination point of the branch also moves right to R_H. Moreover, as $\alpha \to 0$, the imperfect steady states approach the perfect steady states. Therefore, as $\alpha \to 0$, the bifurcation diagram of I becomes that of P, which is shown in Fig. 1. We observe that for R slightly greater than R_0^-, the time evolution of the stable periodic states is "slow" for small α and initially resembles the time evolution of P for R slightly greater than R_H; although in P the trajectories ultimately become unbounded. In addition, both P and I have periodic solution branches which terminate with infinite periods. In P and I these termination points represent heteroclinic and homoclinic orbits, respectively.

An alternative way of bending the vertical Hopf branches of P is to introduce higher-order nonlinear terms in the amplitude equations (see, for example, Ref. 12). Such terms, which are orders of magnitude smaller than the imperfection terms, cannot dominate the response of the system unless the imperfections are negligible in comparison. Thus, if both the imperfection terms and higher-order nonlinear terms are present in the amplitude equations then the effect of the latter may, in general, be only quantitative whereas the effect of the former may dominate the qualitative behavior of the system.

APPENDIX: COEFFICIENTS
IN THE AMPLITUDE EQUATIONS

The coefficients in the amplitude equations (2.6) and (4.1) are defined by

$$a_1 \equiv \frac{Q_{11}}{4cT_0^{1/2}} \left[\frac{l^2 r}{T_0^{1/2}} - 2 \right] , \tag{A1}$$

$$a_2 \equiv \frac{Q_{11}^2}{32cT_0} \left[\sigma^{-2} - \frac{l^4 R_c^0}{T_0} \right] , \tag{A2}$$

$$a_3 \equiv c^{-1} \left[\frac{1}{16} \sigma^{-2} \frac{Q_{21}(Q_{11}+Q_{21})}{T_0} - \frac{1}{8} \frac{l^4 Q_{11}Q_{21}R_c^0}{T_0^2} + f \right] , \tag{A3}$$

$$b_1 \equiv \frac{Q_{21}}{4dT_0^{1/2}} \left[\frac{4l^2 r}{T_0^{1/2}} - 2 \right] , \tag{A4}$$

$$b_2 \equiv \frac{Q_{21}^2}{2dT_0} \left[\frac{\sigma^{-2}}{16} - \frac{l^4 R_c^0}{T_0} \right] , \tag{A5}$$

$$b_3 \equiv d^{-1} \left[\frac{1}{16} \sigma^{-2} \frac{Q_{11}(Q_{11}+Q_{21})}{T_0} - \frac{1}{8} \frac{l^4 Q_{11}Q_{21}R_c^0}{T_0^2} + g \right] , \tag{A6}$$

where

$$c \equiv \frac{\sigma^{-1}}{4} \left[\sigma - 1 + (\sigma+1) \frac{Q_{11}^3}{T_0} \right] , \tag{A7}$$

$$d \equiv \frac{\sigma^{-1}}{4} \left[\sigma - 1 + (\sigma+1) \frac{Q_{21}^3}{T_0} \right] , \tag{A8}$$

$$f \equiv \frac{\sigma^{-1}}{16} \frac{lQ_{11}Q_{21}}{T_0} [3(Q_{12}-Q_{21})\beta - (Q_{32}-Q_{21})\mu] + \frac{1}{16} \left[\frac{l^2 Q_{21} R_c^0}{T_0}(3\gamma+\nu) + \frac{\sigma^{-1}lQ_{21}}{T_0^{1/2}}(3\kappa - \eta) \right]$$
$$- \frac{1}{8} \frac{l^3}{T_0} R_c^0 (3\beta + \mu) + \frac{\sigma^{-1}l}{16}(\mu - 3\beta) , \tag{A9}$$

$$g \equiv \frac{1}{16} \sigma^{-1}l \frac{Q_{11}Q_{21}}{T_0} [(Q_{32}-Q_{11})\mu - 3(Q_{12}-Q_{11})\beta] + \frac{1}{8} \frac{l^2}{T_0} Q_{11} R_c^0 (3\gamma - \nu) + \frac{1}{16} \sigma^{-1}l \frac{Q_{11}}{T_0^{1/2}}(\eta - 3\kappa)$$
$$+ \frac{1}{8} \frac{l^3}{T_0} R_c^0 (3\beta + \mu) + \frac{1}{16} \sigma^{-1}l(3\beta - \mu) , \tag{A10}$$

$$\beta \equiv (Q_{11}^3 - Q_{12}^3 - 3T_0)^{-1} \left[lR_c^0 \left\{ -\frac{l^2}{T_0} \left[\frac{1}{2}(Q_{11}+Q_{21}) + \left[Q_{11} + \frac{Q_{21}}{4} \right] \right] \right\} \right.$$
$$\left. - \frac{3}{2} \sigma^{-1}l(Q_{21}-Q_{11}) + \frac{3}{4} \sigma^{-1}l \frac{Q_{11}Q_{21}}{T_0}(Q_{11}-Q_{21})Q_{12} \right] , \tag{A11}$$

$$\gamma \equiv Q_{12}^{-2} \left\{ -\frac{l^2}{T_0} \left[\frac{1}{2}(Q_{11}+Q_{21}) + \left[Q_{11} + \frac{Q_{21}}{4} \right] \right] - l\beta \right\} , \tag{A12}$$

$$\eta \equiv Q_{32}^{-2} \left[\frac{1}{4} \sigma^{-1}l \frac{(Q_{11}-Q_{21})}{T_0^{1/2}} - 2T_0^{1/2}\mu \right] , \tag{A13}$$

$$\kappa \equiv Q_{12}^{-2} \left[\frac{3}{4} \sigma^{-1}l \frac{(Q_{21}-Q_{11})}{T_0^{1/2}} - 2T_0^{1/2}\beta \right] , \tag{A14}$$

$$\mu \equiv (9Q_{11}^3 - Q_{32}^3 + 5T_0)^{-1} \left[3lR_c^0 \left\{ -\frac{l^2}{T_0} \left[\frac{1}{2}(Q_{11}+Q_{21}) - \left[Q_{11} - \frac{Q_{21}}{4} \right] \right] \right\} \right.$$
$$\left. - \frac{1}{2} \sigma^{-1}l(Q_{11}-Q_{21}) - \frac{1}{4} \sigma^{-1}l \frac{Q_{11}Q_{21}(Q_{11}-Q_{21})Q_{32}}{T_0} \right] , \tag{A15}$$

$$\nu \equiv Q_{32}^{-2} \left\{ -\frac{l^2}{T_0} \left[\frac{1}{2}(Q_{11}+Q_{21}) - \left[Q_{11} + \frac{Q_{21}}{4} \right] \right] - 3l\mu \right\} , \tag{A16}$$

and

$$Q_{mn} \equiv (ml)^2 + n^2 . \tag{A17}$$

For $\sigma = 0.8$, $l = 1$, $T_0 = 31$, and $R_c^0 = 39$, the coefficients take on the values

$$a_1 = 1.086\,393(r/\sqrt{31} - 2) ,$$

$$b_1 = 0.101\,787\,3(4r/\sqrt{31} - 2) , \tag{A18a}$$

$$a_2 = 0.014\,850\,51, \quad b_2 = -0.212\,140\,4 , \tag{A18b}$$

$$a_3 = 188.0945, \quad b_3 = -9.228\,837 . \tag{A18c}$$

The terms I_A and I_B found in the amplitude equation (4.1) are defined by

$$I_A \equiv \frac{lR_c^0}{\pi^2 c T_0^{1/2}} (l^2 I_2 - Q_{11} I_1) ,$$

$$\tag{A19}$$

$$I_B \equiv \frac{lR_c^0}{\pi^2 d T_0^{1/2}} (2l^2 I_4 - Q_{21} I_3) ,$$

where I_1, I_2, I_3, and I_4 are given by

$$I_1 = \pi \int_0^\pi f'(x)\sin x \, dx, \quad I_2 = \pi \int_0^\pi f''(x)\cos x \, dx , \tag{A20}$$

$$I_3 = \pi \int_0^\pi f'(x)\sin(2x)dx, \quad I_4 = \pi \int_0^\pi f''(x)\cos(2x)dx . $$

$$\tag{A21}$$

*Present address: Department of Applied Mathematics 217-50, California Institute of Technology, Pasadena, CA 91125.

†Also at Supercomputer Computations Research Institute and Geophysical Fluid Dynamics Institute, Florida State University, Tallahassee, FL 32306.

[1] J. F. Magnan and E. L. Reiss, SIAM J. Appl. Math. (to be published).

[2] L. Bauer, H. B. Keller, and E. L. Reiss, SIAM Rev. 17, 101 (1975).

[3] E. L. Reiss, SIAM J. Appl. Math. 43, 57 (1983).

[4] T. Erneux and E. L. Reiss, SIAM J. Appl. Math. 43, 613 (1983).

[5] P. Hall and I. C. Walton, J. Fluid Mech. 90, 377 (1979).

[6] H. Kidachi, Prog. Theor. Phys. 68, 49 (1982).

[7] B. J. Matkowsky and E. L. Reiss, SIAM J. Appl. Math. 33, 230 (1977).

[8] J. Tavantzis, E. L. Reiss, and B. J. Matkowsky, SIAM J. Appl. Math. 34, 322 (1978).

[9] E. Knobloch and J. Guckenheimer, Phys. Rev. A 27, 408 (1983).

[10] J. P. Keener, Stud. Appl. Math. 55, 187 (1976).

[11] G. Iooss and W. F. Langford, Ann. N.Y. Acad. Sci. 357, 489 (1980).

[12] J. Guckenheimer and P. Holmes, Nonlinear Oscillations, Dynamical Systems, and Bifurcation of Vector Fields (Springer-Verlag, New York, 1983), p. 404.

[13] M. Golubitsky and D. G. Schaeffer, Singularities and Groups in Bifurcation Theory (Springer-Verlag, New York, 1985), p. 437.

[14] A. M. Soward, Physica D 14, 227 (1985).

[15] A. Libchaber and J. Maurer, in Nonlinear Phenomena at Phase Transitions and Instabilities, edited by T. Riste (Plenum, New York, 1981), pp. 259–286.

[16] K. Buhler and H. Oertel, J. Fluid Mech. 114, 261 (1982).

[17] G. Veronis, J. Fluid Mech. 5, 401 (1959).

[18] G. Veronis, J. Fluid Mech. 31, 113 (1968).

[19] J. Guckenheimer and E. Knobloch, Geophys. Astrophys. Fluid Dynamics 23, 247 (1983).

[20] E. Doedel, Proceedings of the 10th Manitoba Conf. on Num. Math. and Comp. University of Manitoba, Winnipeg, Canada [Congressus Numerantium 30, 265 (1981)].

[21] E. Doedel and J. P. Kernevez, California Institute of Technology Applied Mathematics Report, 1986 (unpublished).